The Spin-up Process of a Cyclone Vortex in a Tropical Cyclone Initialization Scheme and Its Impact on the Initial TC Structure

Chih-Ying Chen[1, 2], Yi-Leng Chen[1], and Hiep Van Nguyen[1, *]

[1]*Department of Meteorology, University of Hawaii at Manoa, Honolulu, HI 96822, USA*
[2]*Institute of Atmospheric Physics, National Central University, Jhongli, Taiwan*

Abstract

The scheme developed by Nguyen and Chen (2011) is used to produce 18 TCs (2004−2013) over the Northwestern Pacific that are well adjusted to the environment. The environment, including SST, in which the storm is embedded has a significant effect on the intensity and rainband patterns of these TCs. During the early season, TCs have a tendency to exhibit a "9" type asymmetric structure with an upper-level outflow channel extending southwestward from the southeastern quadrate of the storm. At low levels, the convergence area between the TC circulation and the southwesterly monsoon flow is a favorable location for the development of spiral rainbands. Late season TCs have a tendency to produce a "6" type storm structure with an outflow channel extending northeastward from the northwestern part of the eyewall, especially when an upper-level cold low or trough is present to the northwest of the storm. At low levels, the convergence of the northeasterly monsoon flow and the TC circulation is favorable for the occurrences of spiral rainbands. For intense TCs that underwent an eyewall replacement cycle, the scheme also shows considerable skill in reproducing the concentric eyewall structure.

(**Citation**: Chen, C., Y. Chen, and H. V. Nguyen, 2014: The spin-up process of a cyclone vortex in a tropical cyclone initialization scheme and its impact on the Initial TC structure. *SOLA*, **10**, 93−97, doi:10.2151/sola.2014-019).

1. Introduction

Tropical cyclone initialization is one of the most challenging problems for the high-resolution numerical weather prediction of tropical cyclones because the TC vortex is not well resolved by the initial conditions provided by global models. There are several initialization methods to produce tropical cyclones in the initial conditions. The first method is to insert and replace the initial vortex from global analysis with an analytic or bogus vortex. This method uses idealized equations to generate a vortex structure in the model initial conditions (Davidson and Weber 2000; Kwon and Cheong 2010). The second method, the bogus data assimilation method, uses variational data assimilation to construct the initial vortex. This method first uses an empirical function to specify TC vortex structure or to generate virtual observations. A variational data assimilation system is then used to assimilate bogus vortex or virtual TC observations and observational data to obtain the best vortex solution as the first guess field (Zou and Xiao 2000; Xiao et al. 2006; Liou and Sashegyi 2012). For the third method, dynamical initialization, the vortex initialization is based on the Newtonian relaxation method and short-time cycle runs are performed to produce the initial TC vortex (Bender et al. 1993; Kurihara et al. 1993; Hendricks et al. 2011).

Nguyen and Chen (2011) (hereafter NC2011) developed a new dynamical TC initialization method using model cycle runs. They hypothesize that the initial TC vortex is closely related to the environmental conditions (including SST) that the storm is embedded in. The initial vortex is spun up by a high-resolution mesoscale model through a series of short (~1 h) cycle runs under given environmental conditions until it reaches or is close to the observed intensity from the best track data. The NC2011 scheme can produce an asymmetric structure of Typhoon Morakot (2009) over the open ocean that is consistent with satellite data. NC2011 compared model simulations from three different initial conditions for Morakot, namely, the initialization using data from the National Centers for Environmental Prediction (NCEP) Global Forecast System (GFS), the Weather Research and Forecasting-Advanced Research WRF (WRF-ARW) model's bogus scheme, and their own scheme. With better initial storm intensity and structure, their scheme's performance in simulating Typhoon Morakot's track and intensity is superior to the other two methods. In addition to Morakot, they also applied their scheme to Typhoon Jangmi (2008) and Kalmaegi (2008). Simulations of four more landfalling TCs over the Northwest Pacific using the NC2011 method were performed by Nguyen and Chen (2014). For all cases considered, the NC2011 scheme shows remarkable skill in improving the track and intensity simulations, especially intensity, over this data sparse region. This is mainly because the initial storm intensity and structure are better adjusted to environmental conditions and well adapted to the model employed.

NC2011 suggests that the asymmetric structure of Morakot over the open ocean with rainbands and convective activity extending from the southeastern quadrat of the eyewall southwestward ("9" type structure) is related to the moisture transport by the southwesterly (SW) monsoon flow and the convergence between the SW monsoon flow and storm circulation. Some of the late summer/early-autumn cases are under the northeasterly (NE) monsoon flow with rainbands and extensive convective activity extending northeastward ("6" type structure). During the mature stage, some storms also undergo an eyewall replacement cycle (Yang et al. 2013). In this study we examine 18 storms, each of which exhibits one of these three types of structure. Are the differences in the storm structure related to the differences in the environmental conditions in which these storms are embedded? Is the initialization technique proposed by NC2011 capable of producing realistic TC structure including radar reflectivity patterns, minimum SLP (P_{min}) and maximum 10-m winds (V_{max}) for all three types of storm? The primary goal of this study is to determine to what extent the NC2011 scheme can reproduce initial TC structure under different environmental settings. The model configuration is given in Section 2. The possible large-scale control on TC structure under different large-scale conditions is investigated in Section 3. The results are summarized in Section 4.

2. Model configuration and vortex spin-up scheme

The global gridded data from NCEP were used as the initial conditions for the vortex spin-up process through a series of 1-h cycle runs in the NC2011 scheme. For each cycle run, the TC vortex at the end of the previous 1-h run is separated from its environmental conditions using the techniques of Kurihara et al. (1993). Because the TC vortex moves during the 1-h integration, the vortex is brought back after integration to its center location, which is determined by the Japanese Meteorological Agency (JMA) best track data for the next 1-h cycle run with the environmental conditions unchanged. The above procedures are repeated until the P_{min} and V_{max} are close to those in the best track data, e.g.,

---

Corresponding author: Yi-Leng Chen, Dept. of Meteorology, SOEST, University of Hawaii at Manoa, Honolulu, HI 96822, USA. E-mail: yileng@hawaii.edu.
* Present affiliation: Hydrology and Environment Vietnam Institute of Meteorology, Vietnam.

P_{min}(NC2011) ~ P_{min}(JMA), or after 80 cycles, whichever comes first. For most cases, both P_{min}(NC2011) and V_{max}(NC2011) are close to the best track data at about Cycle 70.

In NC2011, the SLP associated with the TC vortex is pre-scribed during the cycle runs and is a function of observed P_{min} and storm size (their Eq. 6). However, Nguyen and Chen (2014) show that the prescribed SLP pattern has very little impact on the spin-up process and the final storm structure. Thus, in this study, the SLP is not prescribed. One important assumption used in the NC2011 initialization method is that within the short period of a cycle run, the TC structure and environmental conditions do not change significantly. It is not advisable for the duration of integration for each cycle run to be longer than 3 h because, for most cases, the TC may move into a different environment during this time frame. Cycle runs shorter than 1 h require more com-puting resources with more cycles before P_{min}(NC2011) reaches P_{min}(JMA).

In this paper, the WRF-ARW model v3.3.1 is used. There are two domains with 121 × 121, 205 × 205 grid points and 38 vertical levels[1#] with a grid size of 18 km and 6 km, respectively. As shown in NC2011, a 6-km grid nested in the 18-km domain is adequate to resolve mesoscale structure of TCs. The WSM6 cloud microphysics (Hong and Lim 2006), Grell's cumulus parame-terization (Grell 1993), Rapid Radiative Transfer Model long-wave radiation parameterization (Mlawer et al. 1997), Duhia's shortwave short radiation (Dudhia 1989), and Yonsei University's boundary layer parameterization (Hong and Pan 1996) are em-ployed. The precipitation schemes used are the same as Wu et al. (2012). For the 2004−2006 cases, we use the NCEP Final Analysis (FNL) 1.0-degree data. For the cases after 2007, we use the NCEP GFS data with a 0.5-degree grid. The global SST analysis with a 0.5-degree grid from NCEP is used. A model sensitivity test shows that with SST 28 C within the entire domain for TC Chanchu (2006), the final storm intensity is reduced by 30% (not shown). For each storm, the simulated radar reflectivity pattern is com-pared with microwave observations from satellites. In this paper, three recent examples with "9" type (Soulik 2013), "6" type (Fitow 2013), and concentric eyewall (Chanchu 2006), respectively, are presented to show the capability of the NC2011 scheme.

3. Results and discussion

3.1 "9" type typhoon structure

For the "9" type of tropical cyclone, we selected Typhoon Soulik (2013). The predecessor of Soulik is a mid- to upper-level low about 1,400 km northeast of Guam on 5 July 2013. Soulik formed and was named about 620 km north of Guam at 0000 UTC 8 July 2013. After its formation, Soulik continued to move westward with increasing intensity. At 0000 UTC 10 July, Soulik reached maximum intensity with P_{min} around 925 hPa, about 1000 km southeast of Okinawa. At 0000 UTC 11 July, the low-lev-el circulation patterns are characterized by a moist (Total Precipi-table Water (TPW) 60 mm) southwesterly flow (Fig. 1a) from the ocean north of Indonesia to the southern Philippines. The strong (18 m s^{-1}) (Fig. 1a), moist (TPW 65 mm) southerly flow is present on the eastern/southeastern part of the storm due to large pressure gradients between the storm center and a high-pressure cell to the northeast. Significant confluence is evident between the south-westerly flow and the strong southerly winds on the southeastern/eastern side of the storm (Fig. 1a). Winds on the northwestern/western side of the storms are relatively weak (10 m s^{-1}) and dry (TPW 35 mm). The horizontal structure of Soulik from 85 GHz microwave scattering channel of the Special Sensor Microwave Imager/Sounder (SSMI/S) was asymmetric with a "9" shaped pat-tern (Fig. 2a). Extensive rainbands extended from the eastern side of the typhoon southwestward. The upper-level flow pattern (Fig.
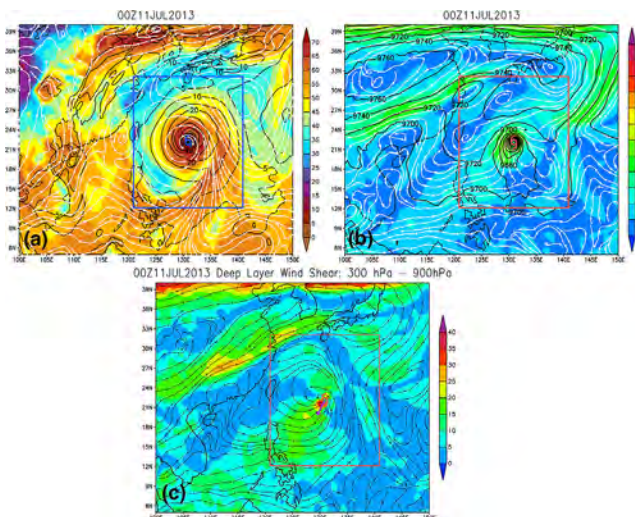

Fig. 1. GFS analysis of Typhoon Soulik (2013) at 0000 UTC, 11 July: (a) 900-hPa level wind speed (contour, m s^{-1}), streamlines, TPW (shaded, mm); (b) 300-hPa geopotential height (contour, m), streamlines, wind speed (shaded, m s^{-1}); and (c) streamlines of 300−900 hPa wind shear vec-tors, wind shear magnitude (shaded, m s^{-1}). The square area denotes the model domain for spin up.
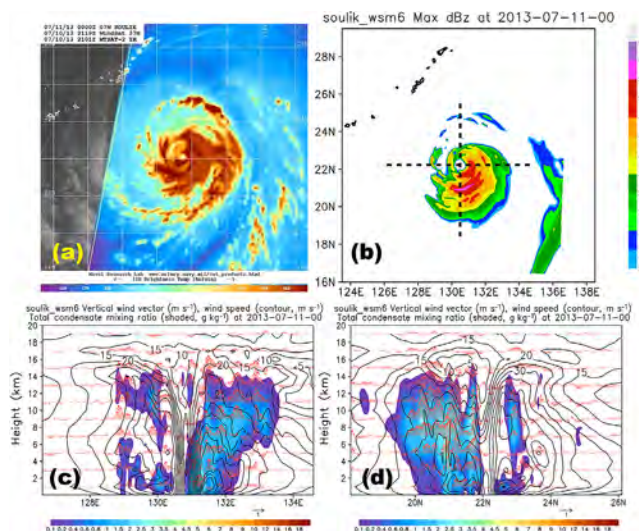

Fig. 2. Typhoon Soulik's structure at 0000 UTC, 11 July 2013: (a) WindSat 37 GHz brightness temperature (degree Kelvin); and (b) simulated radar reflectivity (dBz). The dashed lines indicate the east-west (EW) and north-south (NS) cross sections. (c) The simulated EW cross section across the TC center showing wind speed (contour, m s^{-1}), u component and vertical wind (vector, m s^{-1}), total condensate mixing ratio (shaded, g kg^{-1}). (d) Same as (c) but for the NS cross section.

1b) was characterized by a northeasterly flow with relatively weak winds (5 m s^{-1}) on the southeastern quadrat. A strong outflow channel was located on the south side of the typhoon. The deep layer 300−900 hPa wind shear (Fig. 1c) exhibited a northeasterly wind shear vector (15 m s^{-1}) in the southwestern part of typhoon. Downstream of the environmental wind shear, convection is favored on the left side of the shear vectors (Bender 1997; Frank and Ritchie 2001; Molinari et al. 2004; Rogers et al. 2003).

The simulated radar reflectivity pattern exhibits asymmetric structure (Fig. 2b) consistent with microwave satellite observa-tions (Fig. 2a). In the eastern part of typhoon, the maximum wind speed was 50 m s^{-1} and extended above 5 km with extensive convection. On the western side, however, the simulated maxi-mum wind speed of 50 m s^{-1} along the eyewall is confined to a

---

[1#] Eta levels: 1.000, 0.994, 0.983, 0.968, 0.950, 0.930, 0.908, 0.882, 0.853, 0.821, 0.788, 0.752, 0.715, 0.677, 0.637, 0.597, 0.557, 0.517, 0.477, 0.438, 0.401, 0.365, 0.332, 0.302, 0.274, 0.248, 0.224, 0.201, 0.179, 0.158, 0.138, 0.118, 0.098, 0.078, 0.058, 0.038, 0.018, 0.000.

small area below the 1-km level with relatively weak convective activity (Fig. 2c). In the northern part of typhoon, the maximum wind speed is 50 m s^{-1} and extends above 4 km. On the southern/southeastern side of typhoon, the simulated convective activities are active (Figs. 2c, d).

3.2 "6" type typhoon structure

This type of storm usually occurs in the late season after the onset of the NE monsoon. In this study, we examine the storm structure of Typhoon Fitow. On 26 September 2013, a tropical low-pressure system formed near Palau. On 30 September, it developed into Typhoon Fitow and reached its maximum intensity with P$_{min}$ ~960 hPa at 2100 UTC 4 October. At 1200 UTC 5 October, the 900-hPa level flow was characterized by the presence of northeasterly flow to the north and west of the storm (Fig. 3a). Another storm, TC Danas, was present to the southeast of Fitow. A moisture tongue associated with a mid-latitude cold front north
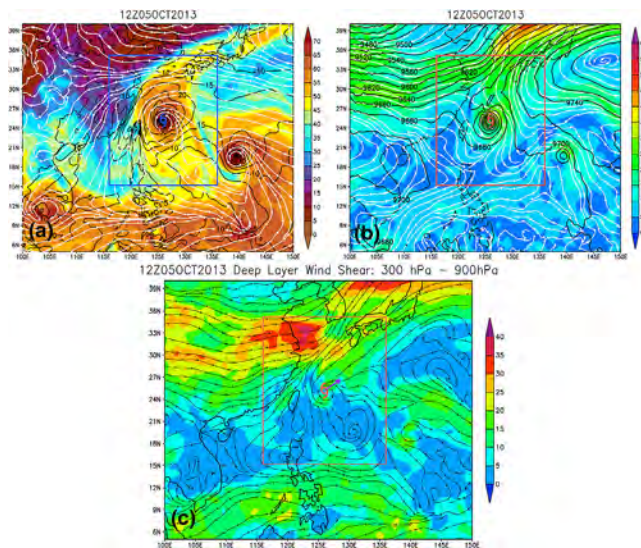

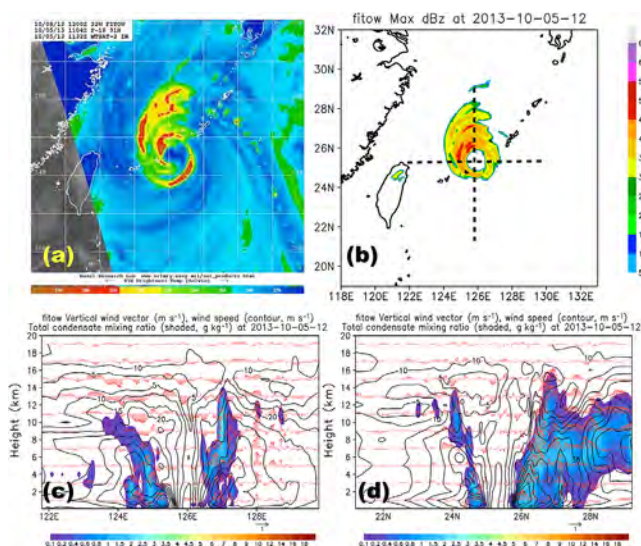Fig. 3. Same as Fig. 1 but for Typhoon Fitow (2013) at 1200 UTC 05 Oct.

Fig. 4. Typhoon Fitow's structure at 1200 UTC 5 October 2013: (a) SSMIS 91 GHz brightness temperature (degree Kelvin); and (b) simulated radar reflectivity (dBz). The dashed lines indicate the east-west (EW) and north-south (NS) cross sections. (c) The simulated EW cross section across the TC center showing wind speed (contour, m s^{-1}), u component and vertical wind (vector, m s^{-1}), total condensate mixing ratio (shaded, g kg^{-1}). (d) Same as (c) but for the NS cross section.

of the typhoon was evident. At the 300-hPa level (Fig. 3b), an outflow channel extended from the storm center to the north and merged with the mid-latitude southwesterly jet. The deep layer wind shear (Fig. 3c) was mainly associated with the mid-latitude baroclinic zone extending northeastward north of the storm center.

From satellite observations (Fig. 4a), the TC exhibited an asymmetric structure with a spiral rainband extending from the northwestern quadrat northeastward. Using the NC2011 technique, the storm structure (Fig. 4b) is consistent with satellite observations (Fig. 4a). Along the East-West cross section (Fig. 4c), the simulated convection activity outside the eyewall is weak because the major moist source is located in the northern part of the typhoon (Fig. 3a). From the north-south cross section (Fig. 4d), the simulated storm exhibits strong tangential winds on the northern side with extensive convective activity associated with the northern spiral rainband (Fig. 4d).

3.3 The concentric eye-wall structure

Typhoon Chanchu formed as a tropical depression on 9 May, 2006 at about 8.3°N, 133.4°E. It made landfall over the Philippines on late 11 May. After Chanchu crossed the Philippines, it intensified into a super typhoon with P$_{min}$ ~920 hPa at 0000 UTC 15 May and underwent an eyewall replacement cycle during 15−16 May. Chanchu occurred after the onset of the SW monsoon over IndoChina with a moisture tongue associated with the southwesterly flow off the southern Vietnam coast extending northeastward off the northwestern Philippines coast (Fig. 5a). Another branch of moist air coming from the south of the western Philippines coast merges with the southwesterly flow. The cyclonic circulation around the storm center is rather symmetric and the relatively drier northerly/northeasterly flow on the western side didn't enter the cyclonic storm circulation. The 300-hPa level weather pattern shows that the westerly jet stream in mid-latitude was located more than 15 degrees northeast of Chanchu (Fig. 5b). An upper-level cold core low was present east of the storm. The upper-level pattern is characterized by a southwesterly flow north of the storm center and a northeasterly flow on the equatorial side. Due to the lack of a strong steering flow, the movement of Chanchu is rather slow[2#] (~4 m s^{-1}) at this time. The deep layer wind shear near the center of the typhoon was weak (5 m s^{-1}) (Fig. 5c), which is favorable for the development of an intense storm (Frank and Ritchie 2001). Furthermore, the vertical wind shear of the horizontal winds also exhibited a north-south symmetry structure with upper-level outflow channels both north and south of the
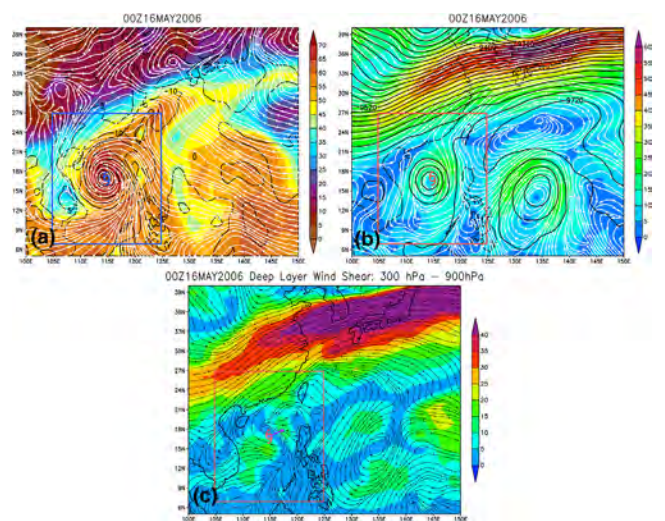

Fig. 5. Same as Fig. 1 but for Typhoon Chanchu (2006) at 0000 UTC 16 May.

————————————————

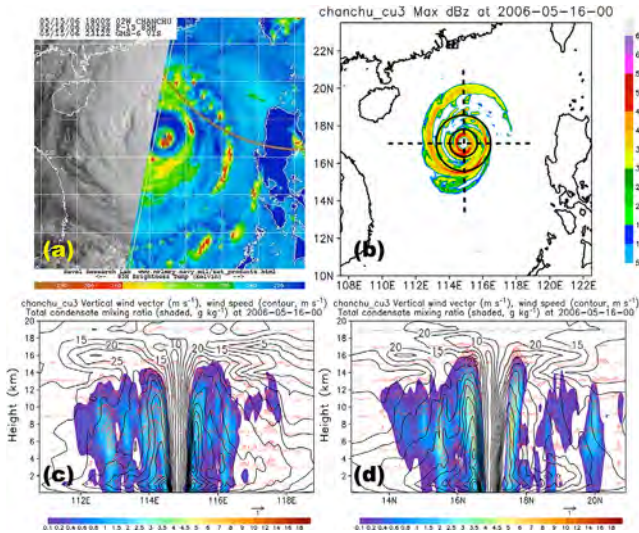[2#] Source: http://www.nrlmry.navy.mil/atcf_web/image_archives/2006/wp 022006.06051600.gif

Fig. 6. Typhoon Chanchu's structure at 0000 UTC, 16 May 2006: (a) The SSMI 85 GHz brightness temperature (degree Kelvin); (b) simulated radar reflectivity (dBz). The dashed lines indicate the east-west (EW) and north-south (NS) cross sections. (c) The simulated EW cross section across the TC center showing wind speed (contour, m s^{-1}), vertical wind (vector, m s^{-1}), total condensate mixing ratio (shaded, g kg^{-1}). (d) same as (c), but for the NS cross section.

storm center.

Satellite observations show that Chanchu has a double eyewall at 0000 UTC 16 May with a symmetric structure (Fig. 6a). The simulated radar reflectivity pattern (Fig. 6b) shows the existence of both the inner and outer eyewall structures with a spiral outer rainband, consistent with satellite observations. Both the east-west and north-south cross sections through the TC center (Figs. 6c, d) also show the double eye wall structure with a much weaker wind speed associated with the outer eyewall. The axisymmetric structure is evident from both the horizontal distribution and vertical cross sections (Figs. 6c, d). With another nested domain with a 2-km grid (not shown), the inner core region of Chanchu is better resolved (Fig. S1). It is apparent that the NC2011 scheme is capable of reproducing the observed concentric eyewall structure after the storm reached the maximum intensity.

We also use the same scheme to spin up other typhoons that occurred in the Northwestern Pacific during 2004−2013 (Table 1, Figs. S2 and S3). For cases embedded in the summer SW monsoon flow with the "9" type asymmetric structure (Dujuan, Nakri, Morakot, Muifa, Jelawat, Vicente, and Trami), the storm structures are reproduced by this scheme. Similarly, cases showing the "6" type structure embedded in the NE monsoon flow (Mitag, Francisco, Lekima, and Krosa) are also successfully spun up in the model with a similar asymmetric storm structure. Typhoon Tembin occurs in late summer but still exhibits a "6" type structure due to the presence of an upper-level cold core to the northwest. Typhoon Haiyan is a wintertime case, but it occurs in low latitude under the southwesterly flow and still exhibits a "9" type structure. In addition to Chanchu, there are other cases (Chaba, Dianmu, and Francisco) that feature eyewall replacement during part of their lifetime. For all the cases considered, our scheme performs reasonably well in duplicating the observed storm structure in the model.

4. Conclusion

Typhoon structure is affected by environmental conditions, including SST. The NC2011 scheme has considerable skill in reproducing the observed structure based on the given environmental conditions in which the storm is embedded.

Under the summer SW monsoon, typhoons have a tendency to

Table 1. All the selected cases from 2004-2013 with the NC2011 typhoon initialization scheme. The first column is the name of the TC. The second column is the spin-up time, and the third column is the TC structure type. "CE" denotes concentric eyewall. Columns 4, 5, and 7 indicate the intensity of the TC from JMA best track, GFS data, and after NC2011 spinup, respectively. The units for P_{min} and V_{max} are hPa and m s^{-1}, respectively. Columns 6 and 8 indicate the error statistics of GFS and NC2011 in comparison with JMA data, respectively. The Mean Absolute Error (MAE) of GFS is 30.2 hPa for P_{min}. The MAE for NC2011 is 2.6 hPa for P_{min}, and 3.3 m s^{-1} for V_{max}.

Name	Time yyyy-mm-dd hhZ	Type	JMA P_{min} V_{max}	GFS P_{min}	GFS Error P_{min}	NC2011 P_{min} V_{max}	NC2011 Error P_{min} V_{max}
Dujuan	2003-08-31 12Z	9	960 36	998	38	961 44	1 8
Nakri	2008-05-31 00Z	9	965 39	1003	38	974 39	9 0
Morakot	2009-08-06 00Z	9	965 34	983	18	966 31	1 3
Muifa	2011-07-31 00Z	9	970 34	991	21	970 35	0 1
Vicente	2012-07-22 00Z	9	990 23	992	2	989 22	1 1
Jelawat	2012-09-23 00Z	9	965 36	992	27	968 40	3 4
Soulik	2013-07-11 00Z	9	935 46	977	42	936 49	1 3
Trami	2013-08-20 00Z	9	970 31	981	11	970 31	0 0
Haiyan	2013-11-05 06Z	9 (special)	980 31	996	16	980 37	0 6
Mitag	2007-11-22 12Z	6	955 41	1001	46	962 40	7 1
Tembin	2012-08-20 12Z	6 (special)	950 41	993	43	960 47	10 6
Fitow	2013-10-05 12Z	6	960 39	980	20	961 39	1 0
Lekima	2013-10-21 18Z	6	980 28	992	12	980 30	0 2
Krosa	2013-11-02 00Z	6	970 41	1000	30	978 37	8 4
Chaba	2004-08-27 06Z	CE	940 41	972	32	944 33	4 8
Dianmu	2004-06-18 12Z	CE	925 49	984	59	925 45	0 4
Chanchu	2006-05-16 00Z	CE	930 49	990	60	930 50	0 1
Fransico	2013-10-22 06Z	CE	945 44	973	28	945 36	0 8

exhibit a "9" type structure with more extensive spiral rainbands extending from the east/southeastern side of the storm southwestward. At low levels, the warm, moist southwesterly flow converges with the cyclonic storm circulation to the south of storm center. With the SW monsoon flow at low levels and equatorial easterlies aloft, the deep layer wind shear tends to be northeasterlies. Under the late season NE monsoon flow, these storms frequently exhibit a "6" type structure with more extensive convection and rainbands extending from the north/northwestern part of the storm center northeastward, in contrast to its southern counterpart. For these late season storms, the TCs are often affected by the mid-latitude frontal systems with southwesterly flow aloft. The low-level cyclonic storm circulation converges with the NE monsoon flow north/northwest of the storm center with upper-level outflow chan-

nel pointing northeastward. It has been shown that the NC2011 TC initialization technique is capable of reproducing both types of asymmetric storm structure. Some intense storms may undergo eyewall replacement during part of their life cycle, especially during the mature stage. The NC2011 scheme also shows considerable skill in reproducing the concentric eyewall structure.

Acknowledgements

Supplement

Figure S1: Results from the 2-km grid for Chanchu (2006).
Figure S2: TC cases showing the "9" type structure.
Figure S3: TC cases showing the "6" and "CE" type structure.

References

Bender, M. A., R. J. Ross, R. E. Tuleya, and Y. Kurihara, 1993: Improvements in Tropical Cyclone Track and Intensity Forecasts Using the GFDL Initialization System. *Mon. Wea. Rev.*, **121**, 2046−2061.

Bender, M. A., R. J. Ross, R. E. Tuleya, and Y. Kurihara, 1997: The Effect of Relative Flow on the Asymmetric Structure in the Interior of Hurricanes. *J. Atmos. Sci.*, **54**, 703−724.

Davidson, N. E., and H. C. Weber, 2000: The BMRC High-Resolution Tropical Cyclone Prediction System: TC-LAPS. *Mon. Wea. Rev.*, **128**, 1245−1265.

Dudhia, J., 1989: Numerical Study of Convection Observed during the Winter Monsoon Experiment Using a Mesoscale Two-Dimensional Model. *J. Atmos. Sci.*, **46**, 3077−3107.

Frank, W. M., and E. A. Ritchie, 2001: Effects of Vertical Wind Shear on the Intensity and Structure of Numerically Simulated Hurricanes. *Mon. Wea. Rev.*, **129**, 2249−2269.

Fujita, T., 1952: Pressure distribution within typhoon. *Geophys. Mag.*, **23**, 437−451.

Grell, G. A., 1993: Prognostic Evaluation of Assumptions Used by Cumulus Parameterizations. *Mon. Wea. Rev.*, **121**, 764−787.

Hendricks, E. A., M. S. Peng, X. Ge, and T. Li, 2011: Performance of a Dynamic Initialization Scheme in the Coupled Ocean–Atmosphere Mesoscale Prediction System for Tropical Cyclones (COAMPS-TC). *Wea. Forecasting*, **26**, 650−663.

Hong, S.-Y., and H.-L. Pan, 1996: Nonlocal Boundary Layer Vertical Diffusion in a Medium-range Forecast Model. *Mon. Wea. Rev.*, **124**, 2322−2339.

Hong, S.-Y., H.-L. Pan, and J.-O. J. Lim, 2006: The WRF Single-moment 6-class Microphysics Scheme (WSM6). *J. Korean Meteor. Soc.*, **42**, 129−151.

Kurihara, Y., M. A. Bender, and R. J. Ross, 1993: An Initialization Scheme of Hurricane Models by Vortex Specification. *Mon. Wea. Rev.*, **121**, 2030−2045.

Kwon, I.-H., and H.-B. Cheong, 2010: Tropical Cyclone Initialization with a Spherical High-Order Filter and an Idealized Three-Dimensional Bogus Vortex. *Mon. Wea. Rev.*, **138**, 1344−1367.

Liou, C.-S., and K. Sashegyi, 2012: On the Initialization of Tropical Cyclones with a Three Dimensional Variational Analysis. *Nat Hazards*, **63**, 1375−1391.

Mlawer, E. J., S. J. Taubman, P. D. Brown, M. J. Iacono, and S. A. Clough, 1997: Radiative Transfer for Inhomogeneous Atmospheres: RRTM, a Validated Correlated-k Model for the Longwave. *J. Geophys. Res.*, **102**, 16663−16616, 16682.

Molinari, J., D. Vollaro, and K. L. Corbosiero, 2004: Tropical Cyclone Formation in a Sheared Environment: A Case Study. *J. Atmos. Sci.*, **61**, 2493−2509.

Nguyen, H. V., and Y.-L. Chen, 2011: High-Resolution Initialization and Simulations of Typhoon Morakot (2009). *Mon. Wea. Rev.*, **139**, 1463−1491.

Nguyen, H. V., Y.-L. Chen, and Y.-L. Chen, 2014: On the Spin-up Process of a Typhoon Vortex in a Tropical Cyclone Initialization Scheme and Its Impacts on the Intensity Simulations. (In Review).

Rogers, R., S. Chen, J. Tenerelli, and H. Willoughby, 2003: A Numerical Study of the Impact of Vertical Shear on the Distribution of Rainfall in Hurricane Bonnie (1998). *Mon. Wea. Rev.*, **131**, 1577−1599.

Wu, C.-C., Y.-H. Huang, and G.-Y. Lien, 2012: Concentric Eyewall Formation in Typhoon Sinlaku (2008). Part I: Assimilation of T-PARC Data Based on the Ensemble Kalman Filter (EnKF). *Mon. Wea. Rev.*, **140**, 506−527.

Xiao, Q., Y.-H. Kuo, Y. Zhang, D. M. Barker, and D.-J. Won, 2006: A Tropical Cyclone Bogus Data Assimilation Scheme in the MM5 3D-Var System and Numerical Experiments with Typhoon Rusa (2002) Near Landfall. *J. Meteor. Soc. Japan*, **84**, 671−689.

Yang, Y.-T., H.-C. Kuo, E. A. Hendricks, and M. S. Peng, 2013: Structural and Intensity Changes of Concentric Eyewall Typhoons in the Western North Pacific Basin. *Mon. Wea. Rev.*, **141**, 2632−2648.

Zou, X., and Q. Xiao, 2000: Studies on the Initialization and Simulation of a Mature Hurricane Using a Variational Bogus Data Assimilation Scheme. *J. Atmos. Sci.*, **57**, 836−860.